Supporting Information

Interlayer Surface Energy Control for High-efficiency Printed Organic Photovoltaic Cells

Jianqiu Wang,[a] Yafei Wang,[a,b] Mengzhen Du,[d] Yue Yu,[a,b] Chaoyi Wang,[a,c] Wenxuan Wang,[a,b] Qing Guo,[d] Yong Cui,[a] Shaoqing Zhang[a,b] and Jianhui Hou[a,b,c]*

[a]State Key Laboratory of Polymer Physics and Chemistry, Beijing National Laboratory for Molecular Sciences, Institute of Chemistry Chinese Academy of Sciences, Beijing 100190, China.

[b]University of Chinese Academy of Sciences, Beijing 100049, China.

[c]School of Chemistry and Biology Engineering, University of Science and Technology Beijing, Beijing 100083, China.

[d]School of Materials Science and Engineering, Henan Institute of Advanced Technology, Zhengzhou University, Zhengzhou 450001, China.

E-mail address: hjhzlz@iccas.ac.cn

Experimental Section

Materials:

PBDB-TF, D18-Cl, PB2, $PC_{71}BM$, IT-4F, BTP-eC9, L8BO, Y6 and FTCC-Br were purchased from Solarmer Materials Inc. PEDOT:PSS (clevios P VP AI 4083) was purchased from H.C. Starck co. Ltd. NDI-Ph was synthesized according to literature.[1] NiO nanoparticles and The glass/ITO substrates were purchased from Huaminxinke Inc. Ag materials were purchased from ZhongNuo Advanced Material (Beijing) Technology Co., Ltd. Other reagents and solvents can be commercial purchased from Innochem or J&K.

OPV cells fabrication:

The OPV cells were fabricated with a structure of ITO/HTL/active layer/NDI-Ph/Ag. PEDOT:PSS was diluted with the same volume of water. NiO nanoparticles were dissolved in water at a concentration of 20.0 mg mL^{-1}. PEDOT:PSS:NiO were prepared with a 1.0:1.0 volume of PEDOT:PSS and NiO nanoparticles aqueous solution. NDI-Ph was dissolved in methanol at a concentration of 1.5 mg mL^{-1}. The PBQx-TCl:eC9-2Cl (wt/wt, 1.0:1.2) was dissolved in toluene with a concentration of 8.0 mg mL^{-1} with respect to the polymer. 0.5% 1,8-diiodooctane (DIO) was added to the solutions before the blade-coating process. The PBDB-TF:$PC_{71}BM$ (wt/wt, 1.0:1.0) was dissolved in chlorobenzene (CB) with a concentration of 10.0 mg mL^{-1} with respect to the polymer. 1.0% DIO was added to the solutions. The PBDB-TF:IT-4F (wt/wt, 1.0:1.0) was dissolved in CB with a concentration of 10.0 mg mL^{-1} with respect to the polymer. 0.5% DIO was added to the solutions. The PBDB-TF:BTP-eC9 (wt/wt, 1.0:1.2) was dissolved in CB with a concentration of 8 mg mL^{-1} with respect to the polymer. 0.5% DIO was added to the solutions. The PBDB-TF:L8-BO (wt/wt, 1.0:1.2) was dissolved in CF with a concentration of 7.5 mg mL^{-1} with respect to the polymer. 0.25% DIO was added to the solutions. The D18:Y6 (wt/wt, 1.0:1.4) was dissolved in CF with a concentration of 6.0 mg mL^{-1} with respect to the polymer. The PB2:BTP-eC9 (wt/wt, 1:1.2) was dissolved in CB with a concentration of 9.0 mg mL^{-1} with respect to the polymer. 0.5% DIO was added to the solutions. The PB2:FTCC-Br:BTP-eC9 (wt/wt, 1.0:0.2:1.0) was dissolved in CB with a concentration of 9.0 mg $mL^{-1}$with respect to the polymer. 0.5% DIO was added to the solutions. The active layer solutions need to be stirred for 3 h. The OPV cells were prepared according to the following procedure. The pre-cleaned ITO substrates were subjected to UV-ozone treatment for a duration of 15 minutes, following which HTL was blade-coated onto their surface. The HTLs were blade coated onto the ITO substrates at a coating speed (U) of 2 mm s^{-1} and a substrate temperature of 50 °C with the gap between the substrate and the blade being 100 μm. Then, the HTLs were annealing at 160 ℃ for 10 min. All the samples were transferred into N_2 glove box for further process. Then the active layer solutions were blade-coated, and annealed at 100 ℃ for 10 minutes (active layer PBDB-TF:$PC_{71}BM$ does not require annealing). The active layer inks were blade coated onto the ITO substrates at a U of 3.0 mm s^{-1} with the gap between the substrate and the blade being 100 μm. Subsequently, NDI-Ph solution was blade coated on surface of active layer. After that, 100 nm of Ag cathode were thermally evaporated under high vacuum (ca. 1×10^{-5} Pa). The device area, as defined by the overlap of ITO and Ag,

are 1.112 cm^2, and corresponding length and width are 1.39 cm and 0.80 cm, respectively. The area of aperture is 1.026 cm^{-2}.

Large-area OPV module fabrication:

The large-area OPV modules with the structure glass/ITO/HTL/active layer/NDI-Ph/Ag and PET/ITO/HTL/active layer/NDI-Ph/Ag were fabricated via blade coating. Patterned ITO substrates (P1 = 120 μm) were purchased from Huananxiangcheng Inc. The ITO substrates were cleaned using the above method. The HTLs were blade coated onto the ITO substrates at a coating speed (U) of 2 mm s^{-1} and a substrate temperature of 50 °C with the gap between the substrate and the blade being 100 μm. The coated films were annealed at 120 °C for 10 min. Then, the PBQx-TCl:eC9-2Cl solution with a concentration of 8 mg ml^{-1} was blade coated on top of the glass/ITO/PEDOT:PSS:NiO and PET/ITO/PEDOT:PSS:NiO structures. The active layer solution was blade coated at U = 3.0 mm s^{-1} and a gap between the substrate and the blade was 150 μm. Subsequently, the substrates containing the active layer was transferred to a nitrogen-purged glove box and annealed at 100 °C for 10 min. Then, the NDI-Ph layer was coated. The P2 pattern was created using a mechanical scribing machine. For the modules of glass/ITO substrate, the samples were transferred to the thermal evaporator again, and a 150-nm-thick Ag layer was deposited. Then, the P3 patterns were created using the mechanical scribing machine. Notably, to prevent the etched Ag from sticking and causing a short circuit, an air knife was used during the etching process. For the modules of PET/ITO substrate, the samples were transferred to the thermal evaporator again, and a 150-nm-thick Ag layer was deposited through a shadow mask. The rigid module contained a 0.469-mm-wide dead zone in each sub-cell (as shown in **Figure S19**), and the GFF was calculated as: photoactive area/overall module area × 100% = [(47.4 mm – 0.469 mm × 6) × 50 mm]/(47.4 mm × 50 mm) × 100% = 94%. The flexible module contained a 1.27-mm-wide dead zone in each sub-cell (as shown in **Figure S19**), and the GFF was calculated as: photoactive area/overall module area × 100% = [(55.65 mm – 1.27 mm × 7) × 58 mm]/(55.65 mm × 58 mm) × 100% = 84%.

Device characterization and measurements:

The *J-V* characteristics of solar cells were recorded with a Keithley 2400 source meter unit under standard AM 1.5G (100 mW cm^{-2}) solar irradiation sourced via a solar simulator (SS-F5-3A, Enlitech Technology CO., Ltd.) The AM 1.5G light source with a radiative intensity of 100 mW cm^{-2} was calibrated by a standard silicon solar cell (SRC-2020), this standard cell was calibrated by the National Institute of Metrology (NIM), China. The cells were characterized at room temperature in glove box filled under a N_2 atmosphere. The EQE data were obtained from a solar cell spectral response measurement system (QE-R3011, Enlitech Technology Co. Ltd). EQE_{EL} and EL spectra were collected through the devices (ELCT-3010, Enlitech). Photo-CELIV mobilities, TPV data and Charge extraction data were obtained by the all-in-one characterization platform, Paios (Fluxim AG, Switzerland). The UPS measurements were performed on the Bruker ESCALAB250Xi system. GIWAXS were measured on a Xeuss 2.0 SAXS/WAXS system (Xenocs SA, France). Cu Kα X-ray source (GeniX3D Cu ULD), generated at 50 kV and 0.6 mA, was utilized to produce X-ray radiation with a wavelength of 1.5418 Å. A semiconductor detector (Pilatus 300 K, DECTRIS, Swiss) with a resolution of 487 × 619 pixels was used to collect the scattering signals. The incident angles are 0.19-0.21°. The

EQE mapping measurements were carried out by using LSD4 system (Enlitech). The instrument was equipped with 520 nm lasers.

Contact angle measurement:

Contact angles and surface tension of different solvents on the active layer films were measured by using a KRÜSS Drop shape analyzer- DSA100. For moving contact angle measurements, the substrate was controlled by a moving platform with moving speed of 3.0 mm/s.

Viscosity measurement:

Viscosities were determined using an Ubbelohde viscometer with a viscometer constant of 0.002787 at 25°C, and the viscometer constant was calibrated with 1,2-ethanediol. For measurements conducted at 25°C, the viscometer was immersed in a temperature controlled water bath. Solutions were allowed to equilibrate at the preset temperature for 15 min before analysis, and viscosity values were averaged over five runs.

PFQNM measurement:

Atomic force microscopy (Bruker Nanoscope V) was employed to analyze the surface topography and modulus of films. AFM cantilevers made of Antimony doped silicon (model: RTESPA-300) were purchased from Bruker. The back-side coating of the cantilever was reflective Al. The Si-tips used had a resonance frequency of about 300 kHz and a spring constant of about 40 N m^{-1}. The scan rate was 1 Hz. The films were prepared with the same as those used in device fabrication. The height and phase images were measured in tapping mode and the scanning area was 2 μm×2 μm. The elastic moduli of the films were measured by peak force quantitative nanomechanical mapping (PFQNM) mode. The mechanical properties were measured at the peak force setpoint of 40 nN by a probe (RTESPA-300) with k = 28.2 N/m.

TPC measurement:

TPC measurements were performed by applying a 488 nm solid-state laser (Coherent OBIS CORE 488LS) with a pulse width of ~30 ns. The decay traces were recorded by a mixed domain oscilloscope (Tektronix MDO3032).

Determinations of energy level and work function:

The highest occupied molecular orbitals (HOMO) and work function are calculated from the spectrum obtained by UPS. The secondary electron onset value (E_{cutoff}), the valence band maximum value (E_{VBM}), and the energy of He I ($h\nu$) was used to calculate the ionization potential (IP, IP value is the inverse of HOMO value) by applying the Equation S1.

$$E_{HOMO} = -IP = -(\emptyset + E_{VBM}) = -(h\nu - E_{cutoff} + E_{VBM}) \#Equation\ S1$$

E_{cutoff} is obtained by onset point from the cross point between two trend lines (one is placed on the baseline and the other on the slope of the peak). The Fermi energy level (E_F) of neat films was calculated by follow equation,

$E_F = h\nu - (E_{F,Au} - E_{cutoff})\#Equation\ S2$

where $E_{F,Au}$ is the Fermi energy level (E_F) of gold. $E_{F,Au}$ is 20.97 eV in this work. Optical gaps (E_g) were determined from the onset of UV-visible absorption spectra. The $E_{g,opt}$ corresponds to the lowest gap between the lowest occupied molecular orbital band (LUMO) and HOMO. Tauc plots of the three HTLs were generated based on absorbance spectra using following equation:

$$(AE)^{1/n} = B(E\text{-}E_g) \qquad \text{Equation S3}$$

where A, E and B represent absorbance, photon energy and constant, respectively. Photon energy E is defined as $E = hc/\lambda$, where h is Planck's constant and c is the speed of light, λ is wavelength.

Film formation kinetics analysis:

In-situ fast response ultraviolet visible absorption spectroscopy measurements were performed by the OCEAN-FX-VIS-NIR-ES spectrometer. The HL-2000-FHSA light source is purchased from Ocean Optics Inc. In-situ Photoluminescence Spectra Measurements were performed by a laser device (LSM-365A, Ocean Optics Inc) with time resolution of 0.1s. The excitation wavelength was 365 nm.

Photophysics characterizations:

TA spectra were measured by the Ultrafast Helios pump-probe system in conjunction with a regenerative amplified laser system from Coherent. A Ti:sapphire amplifier (Astrella, Coherent) was used to generate an 800 nm pulse with a repetition rate of 1 kHz, a length of 100 fs, and an energy of 7 mJ pulse^{-1}. Then, the 800 nm pulse was separated into two parts by a beam splitter. One part was coupled into an optical parametric amplifier (TOPAS, Coherent) to generate the pump pulses at various wavelengths. The other part was focused onto a sapphire plate and a YAG plate to generate white light supercontinuum as the probe beams. The spectral ranges of the probe beams were 420-800 nm and 750-1600 nm, respectively. The time delay between the pump and probe was controlled by a motorized optical delay line with a maximum delay time of 8 ns. The sample films were blade-coated onto the quartz plates and prepared to resist water and oxygen in air, the samples were encapsulated by epoxy resin in N_2 filled glove box. The pump pulse was chopped by a mechanical chopper at 500 Hz and then focused onto the mounted sample with probe beams. The probe beam was collimated and focused into a fiber-coupled multichannel spectrometer with a CCD sensor. The energy of the pump pulse was measured and calibrated by a power meter (PM400, Thorlabs). To avoid exciton-exciton and exciton-charge annihilation effects, the excitation densities of the lasers used for TA measurements were kept as low as 10 μJ cm^{-2}.

Stability measurements:

The cells were encapsulated by exposing epoxy resin to a 365 nm UV lamp for 10 min and further tested white LED light, 100 mW cm^{-2}. The photostability test system is placed in a temperature room of 20 °C, and the multiple radiator fans are applied to the photostability test system to ensure a constant temperature of ~50 °C and the relative humidity is about 40%.

Substrate Surface Energy Determination:

Based on the Young's Equation1, the contact angle of a pure liquid droplet on a smooth and chemically homogenous solid surface at thermodynamic equilibrium is defined as the balance of three interfacial tensions (Figure 1A and Equation S4):

$\gamma_s = \gamma_{sl} + \gamma_l cos\theta \#Equation\ S4$ are γ_l, γ_{sl} and γ_s are liquid-vapor, solid-liquid and solid-vapor interfacial free energies respectively, and θ is the static contact angle (often quasi-static advancing contact angle is used). Liquid-air interfacial free energy of the pure probing liquid (γ_l) and contact angle (θ) can be measured using the pendant and sessile drop methods and axisymmetric drop shape analysis using standard Goniometers. However, one equation is insufficient for determining two unknowns, γ_{sv} and γ_{sl}. It has been shown experimentally that γ_{sv}, γ_{sl} and γ_{lv} are not independent states of the system, but are related via an equation of state. In other words, γ_{sl} can be fully determined by γlv and γsv (assuming the system is in thermodynamic equilibrium),

$\gamma_{sl} = f(\gamma_s, \gamma_l) \#Equation\ S5$

Specifically, we employ the following equation-of-state relation in our work:

$\gamma_{sl} = \gamma_{lv} + \gamma_{sv} - 2\sqrt{\gamma_{lv}\gamma_{sv}\left(1 - \beta(\gamma_{lv} - \gamma_{sv})^2\right)} \#Equation\ S6$

where β is an empirical constant. The $\gamma_l + \gamma_s - 2\sqrt{\gamma_l \gamma_s}$ term comes from the geometric mean combining rule, which is rooted in London theory of dispersion and assumes one dominant type of interactions between the liquid and the solid molecules, or like pairs. However, the combining rule overestimates the interaction between two dissimilar pairs (unlike pairs) and an empirical parameter ($1-\beta(\gamma_l-\gamma_s)^2$) is added to correct for this deviation from experimental results, while maintaining the symmetry of combining rules. By combining Equation S3 with the Young's equation (Equation S1), $cos\theta$ can be expressed as,

$$cos\theta = -1 + 2\sqrt{\frac{\gamma_s}{\gamma_l}}\left(1 - \beta(\gamma_l - \gamma_s)^2\right) \#Equation\ S7$$

By measuring contact angles (θ) with a series of probing liquids with known but diverse surface energies (γ_l), substrate surface energy (γ_s) and β specific for each substrate can be calculated using the least squares regression method.

Measurements and calculations of spreading coefficient

Spreading coefficients (S) for the coatings on the plastisol substrates are calculated as:

$$S = \gamma_S - \gamma_L - \gamma_{SL} \qquad Equation\ S8$$

The theory of describe interactions between solid surfaces and liquids is based on Good's equation. The equation is as follows:

$$\gamma_{SL} = \gamma_S + \gamma_L - 2\left(\gamma_L^D \gamma_S^D\right)^{\frac{1}{2}} - 2\left(\gamma_L^P \gamma_S^P\right)^{\frac{1}{2}} \quad Equation\ S9$$

where γ_L is surface tension of the liquid, γ_L^D is dispersive component of the surface tension of the liquid, γ_L^P is polar component of the surface tension of the liquid, γ_S is overall surface free energy of the solid, γ_S^D is dispersive component of the surface free energy of the solid, γ_S^P is polar component of the surface free energy of the solid. Here, the γ_L^D and γ_L^P is as follows:

$$\gamma_L^D = \frac{\gamma_L^2 (cos\theta_{PTFE} + 1)^2}{72} \quad Equation\ S10$$

$$\gamma_L^P = \gamma_L - \gamma_L^D \quad Equation\ S11$$

where θ_{PTFE} is contact angle measured between PTFE and probe liquid. The γ_S^D or γ_S^P can be calculated by measuring the contact angle between that the polar or dispersive liquid (*ie.* water and diiodomethane) and surface of solid.

Recombination rate constant calculation:

The relationship between n and τ is determined using the equation:

$\tau = \tau_0 n^{-\lambda} \#Equation\ S12$

where τ_0 is constant and λ is the recombination exponent. The recombination order can be determined based on $R = \lambda+1$. The bimolecular recombination rate constants k_{rec} are calculated from τ and n according to the formula:

$$k_{rec} = \frac{1}{(\lambda+1) n \tau(n)} \#Equation\ S13$$

Determinations of voltage losses:

The voltage losses in photovoltage cell can be categorized into three contributions:

$$\Delta V = \frac{E_g}{q} - V_{oc} = \left(\frac{E_g}{q} - V_{OC}^{SQ}\right) + \left(V_{OC}^{SQ} - V_{OC}^{rad}\right) + \left(V_{OC}^{rad} - V_{OC}\right) = \Delta V_1 + \Delta V_2 + \Delta V_3 \quad \text{Equation S1}$$

The E_g value is determined by the derivatives of the Fourier transform photocurrent spectroscopy (EQE_{FTPS}) curve and then calculated with the following equation:

$$E_g = \frac{\int_a^b E_g P(E_g) dE_g}{\int_a^b P(E_g) dE_g} \quad \text{Equation S14}$$

V_{OC}^{SQ} is the maximum voltage based in the Shockley-Queisser (SQ) limit, where the EQE_{PV} is assumed to be a step-function, i.e., 1 above the gap and 0 below the gap. In SQ limit, V_{OC}^{SQ} follows

$$V_{OC}^{SQ} = \frac{KT}{q} \ln\left(\frac{J_{SC,SQ}}{J_{0,SQ}} + 1\right) = \frac{KT}{q} \ln\left(\frac{q\int_{Eg}^{\infty} \emptyset_{AM1.5}(E) dE}{q\int_{Eg}^{\infty} \emptyset_{bb}(E) dE} + 1\right) \quad \text{Equation S15}$$

where $\emptyset_{AM1.5}$ is the solar radiation photo flux, $\emptyset_{bb}$ is a black body radiation at 300K. V_{OC}^{rad} is the voltage where the all recombination is radiative (i.e., EQE_{EL}=1), and follows from

$$V_{OC}^{rad} = \frac{KT}{q}\ln\left(\frac{J_{SC,rad}}{J_{0,rad}} + 1\right) = \frac{KT}{q}\ln\left(\frac{q\int_{Eg}^{\infty} EQE_{PV}\emptyset_{AM1.5}(E)dE}{q\int_{Eg}^{\infty} EQE_{PV}\emptyset_{bb}(E)dE} + 1\right)$$ Equation S16

The voltage loss due to non-radiative recombination can be obtained by:

$$\Delta V_{OC}^{non-rad} = V_{OC}^{rad} - V_{OC}$$ Equation S17

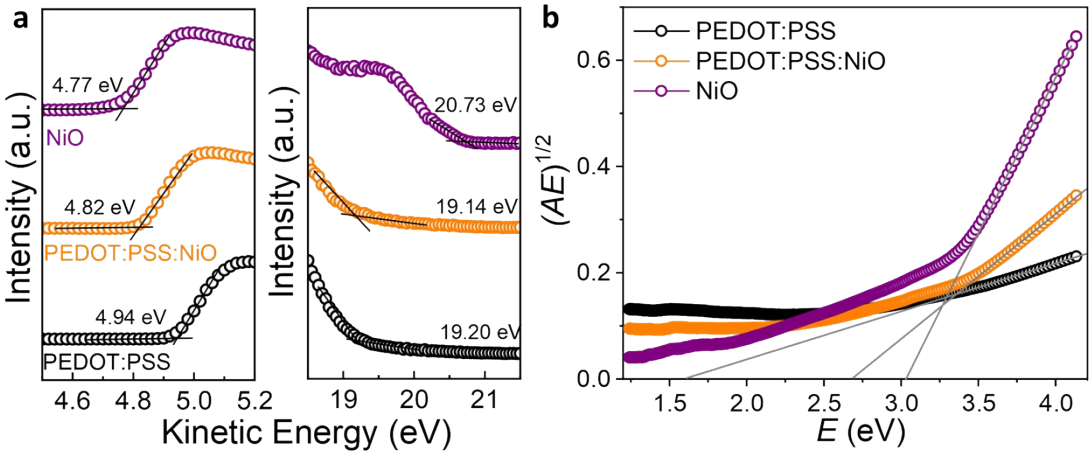

Figure S1. **a.** UPS results and **b.** Tauc plots of neat PEDOT:PSS, PEDOT:PSS:NiO and NiO films.

Table S1. Probing liquids and their surface tensions at ambient temperature.

Probing Liquid	Surface Tension (mN/m)[a]
Formamide	59.1
Glycerol	65.0
Water	72.7
hydrogen peroxide	78.9
Mercury	470

The data obtained from literature.[2]

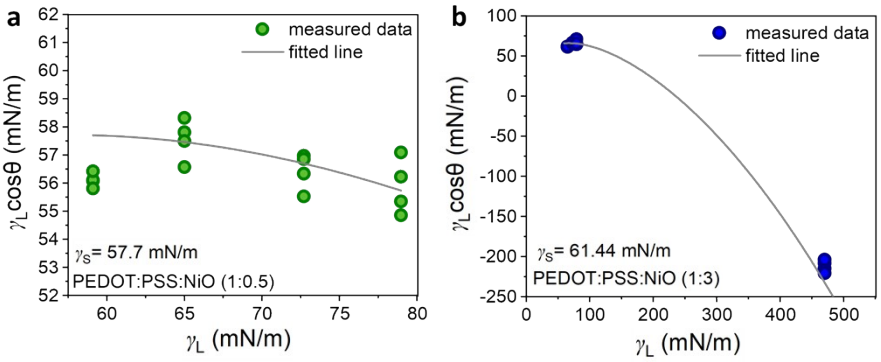

Figure S2. The $\gamma_L\cos\theta$ versus γ_L of a PEDOT:PSS:NiO HTL with volume ratio of **a.** 1:0.5 and **b.** 1:3.

Table S2. Advancing contact angles of the probing liquids on various substrates.

	PEDOT:PSS	PEDOT:PSS:NiO (1:0.5)	PEDOT:PSS:NiO (1:1)	PEDOT:PSS:NiO (1:3)	NiO
Formamide	25.82±0.46	/	/	/	/
Glycerol	36.01±0.42	18.29±0.67	19.27±0.19	18.12±0.56	/
Water	45.36±0.27	27.67±1.20	32.90±0.16	23.85±0.22	19.05±0.11
hydrogen peroxide	50.36±0.16	39.08±0.71	40.175±0.15	32.42±3.86	24.65±0.33
Mercury	/	44.95±0.88	/	116.8±0.87	121.07±0.71

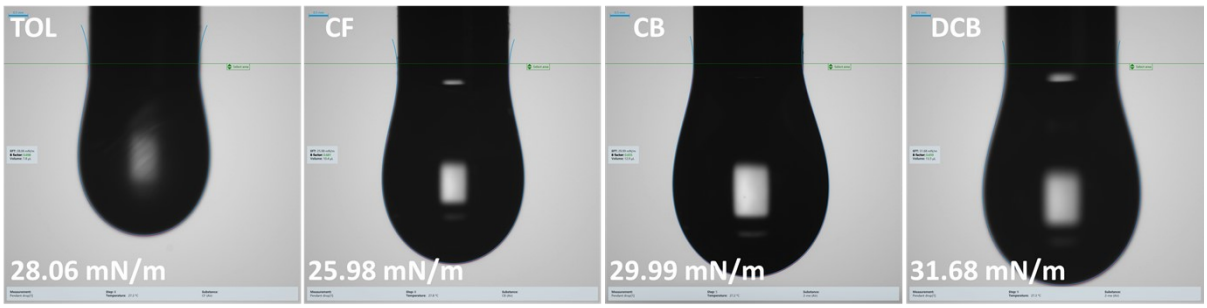

Figure S3. Surface tension of TOL, CF, CB and DCB solvents.

Figure S4. Contact angle images of TOL, CF, CB and DCB solvents on PTFE film.

Table S3. The calculation parameters of the interfacial tension between the solvents and HTLs.

Solvents	HTLs	γ_S (mN m^{-1})	γ_L (mN m^{-1})	γ_L^D (mN m^{-1})	γ_S^D (mN m^{-1})	γ_L^P (mN m^{-1})	γ_S^P (mN m^{-1})	γ_{SL} (mN m^{-1})
TOL	PEDOT:PSS	53.35	28.06	25.15	39.61	2.91	13.74	22.76
	PEDOT:PSS:NiO	61.44	28.06	25.15	43.71	2.91	17.73	24.71
	NiO	70.30	28.06	25.15	46.01	2.91	24.29	25.78
CF	PEDOT:PSS	53.35	25.98	23.59	39.61	2.39	13.74	23.86
	PEDOT:PSS:NiO	61.44	25.98	23.59	43.71	2.39	17.73	26.08
	NiO	70.30	25.98	23.59	46.01	2.39	24.29	27.43
CB	PEDOT:PSS	53.35	29.99	25.39	39.61	4.59	13.74	18.99
	PEDOT:PSS:NiO	61.44	29.99	25.39	43.71	4.59	17.73	20.64
	NiO	70.30	29.99	25.39	46.01	4.59	24.29	21.53
DCB	PEDOT:PSS	53.35	31.68	27.58	39.61	4.09	13.74	20.62
	PEDOT:PSS:NiO	61.44	31.68	27.58	43.71	4.09	17.73	22.13
	NiO	70.30	31.68	27.58	46.01	4.09	24.29	22.76

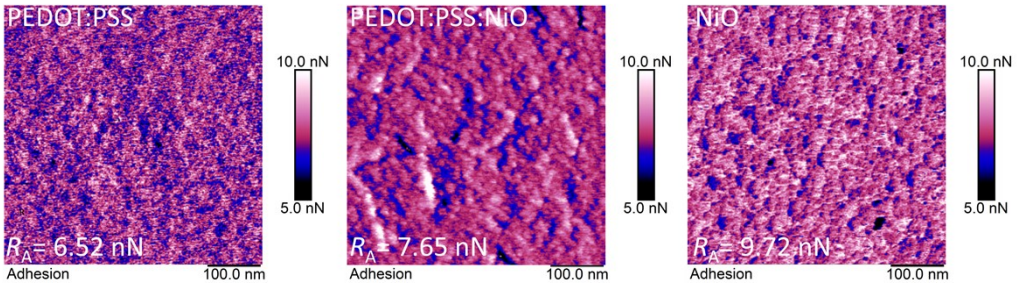

Figure S5. PFQNM adhesion patterns of PEDOT:PSS, PEDOT:PSS:NiO and NiO HTLs.

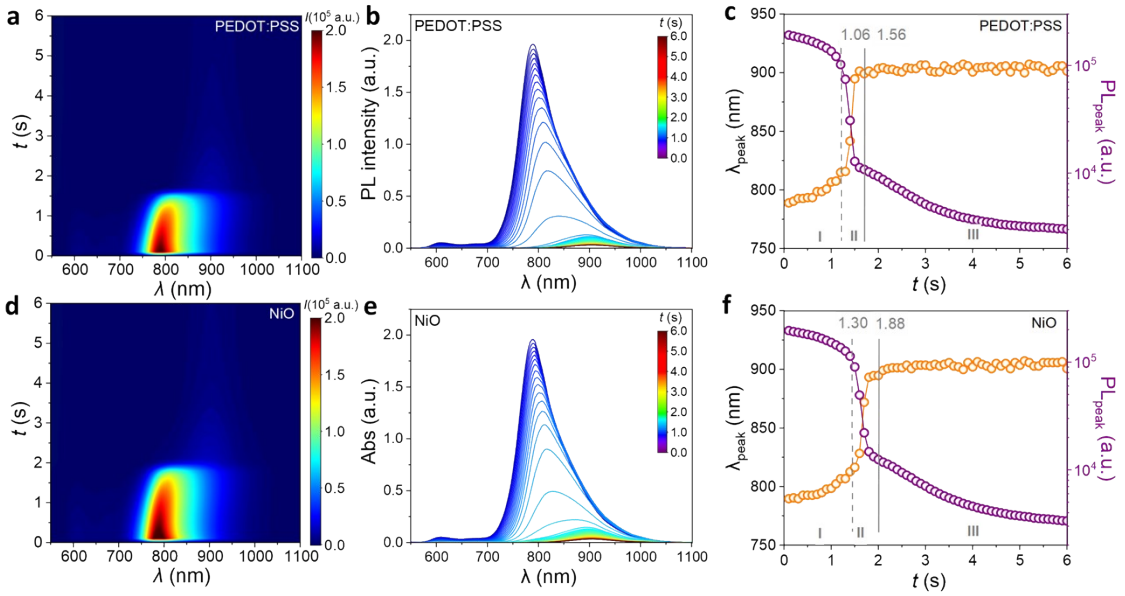

Figure S6. **a,d.** Time-dependent contour maps and **b**,**e.** line-cuts of in-situ PL spectra of PEDOT:PSS and NiO, respectively. **c**,**f.** Time evolution of intensity and peak location of in-situ PL spectra of PEDOT:PSS and NiO.

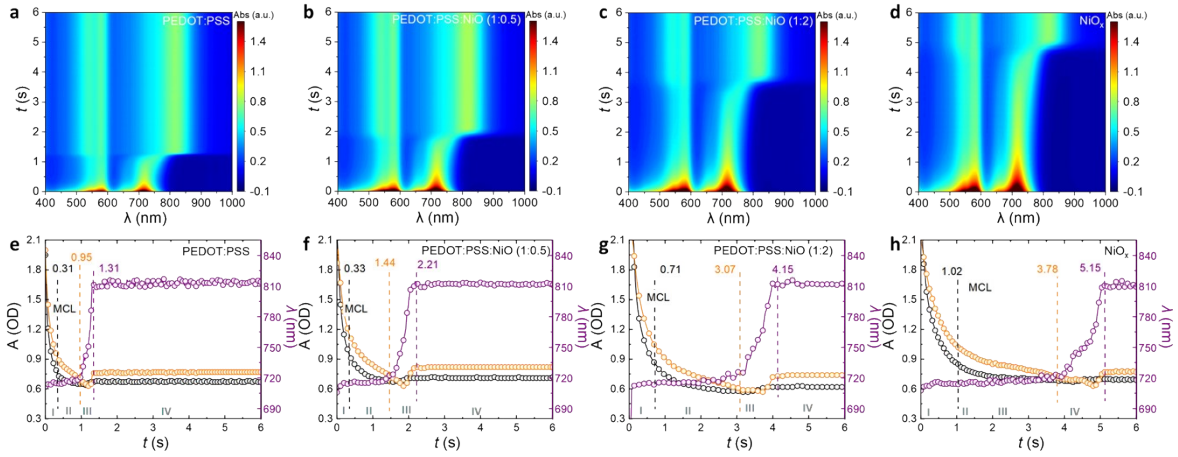

Figure S7. **a-d.** Time-dependent contour maps of in-situ UV-vis absorption spectra of PBQx-TCl:eC9-2Cl ink blade coated on various HTLs. **e-f.** Time evolution of intensity and peak location of in-situ UV-vis absorption spectra of PBQx-TCl:eC9-2Cl ink blade coated on variousHTLs.

Table S4. The parameters for L_p calulations.

ink	μ (mp s)	γ_{LG} (mN/m)	ϕ	U (mm/s)	g (N/kg)
PBQx-TCl:eC9-2Cl	0.63	35.49	0.0167	3.0	9.8
PBDB-TF:BTP-eC9	0.56	25.59	0.0167	3.0	9.8
D18-Cl:Y6	0.60	32.44	0.0167	3.0	9.8
PB2:BTP-eC9	0.46	20.77	0.0167	3.0	9.8

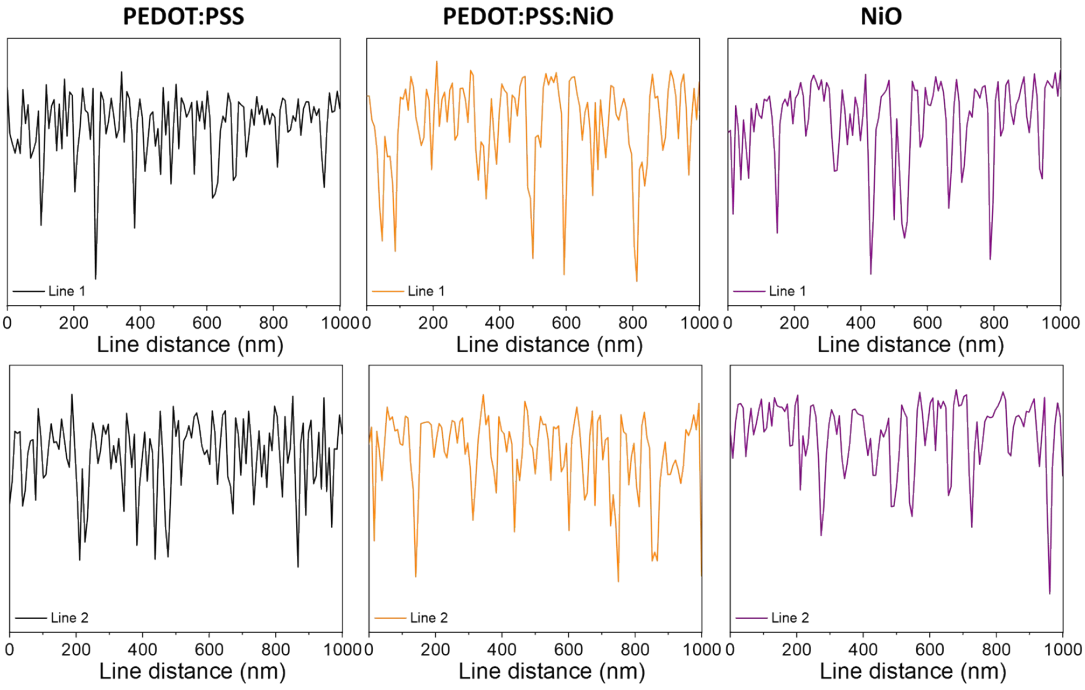

Figure S8. The line profiles to obtain the FWHM of cross-sections though AFM signals of PBQx-TCl:eC9-2Cl coated on PEDOT:PSS, PEDOT:PSS:NiO and NiO HTLs.

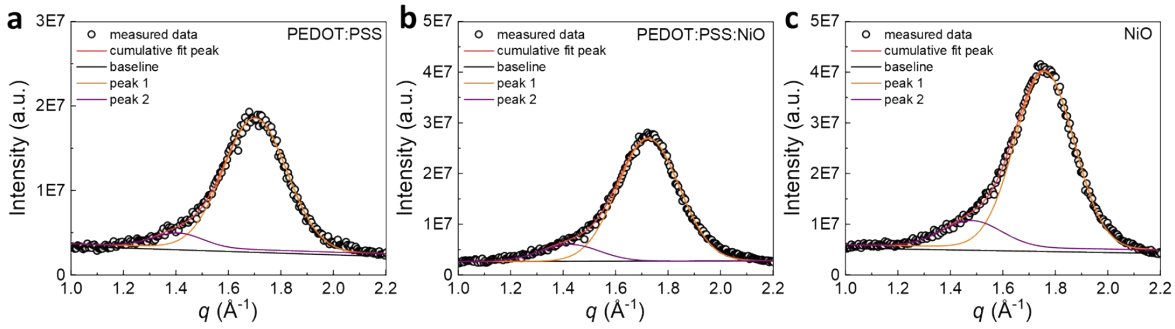

Figure S9. Line-cut profiles in the out-of-plane directions of PBQx-TCl:eC9-2Cl coated on the three HTLs.

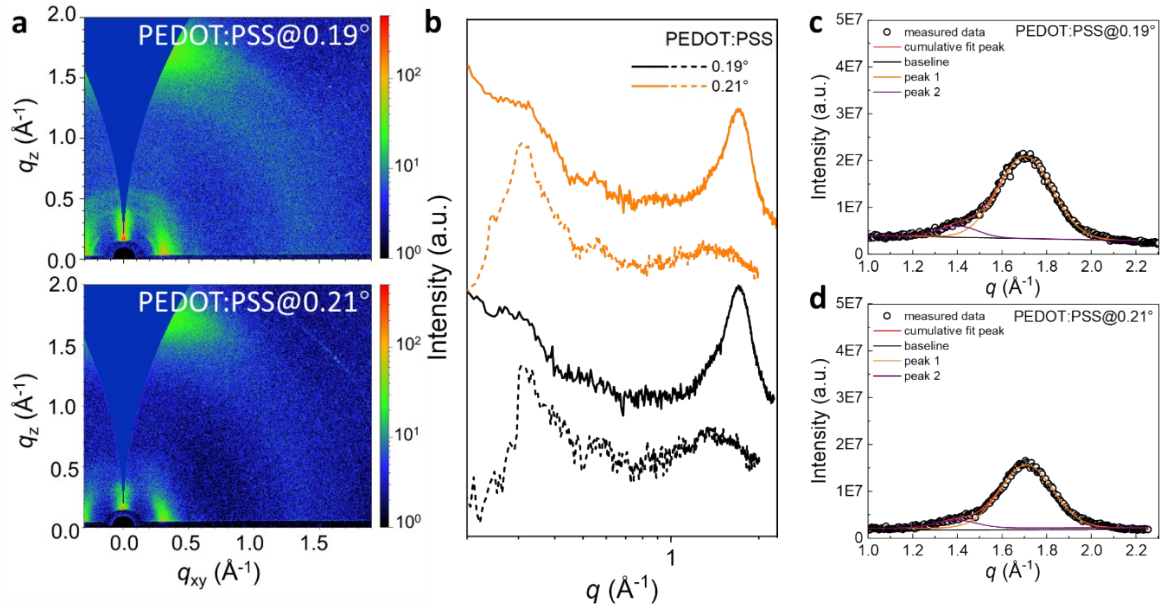

Figure S10. a. 2D GIWAXS patterns, **b.** corresponding 1D line-cue profiles and **c-d.** fitting results of at different X-ray incident angles for PBQx-TCl:eC9-2Cl coated on PEDOT:PSS HTL.

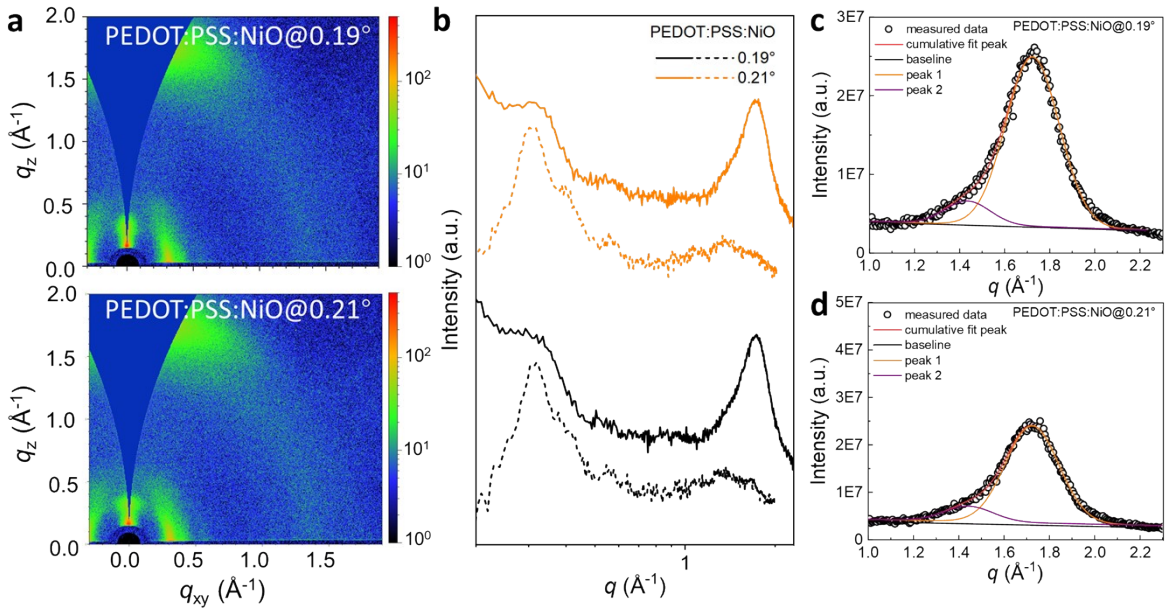

Figure S11. a. 2D GIWAXS patterns, **b.** corresponding 1D line-cue profiles and **c-d.** fitting results of at different X-ray incident angles for PBQx-TCl:eC9-2Cl coated on PEDOT:PSS:NiO HTL.

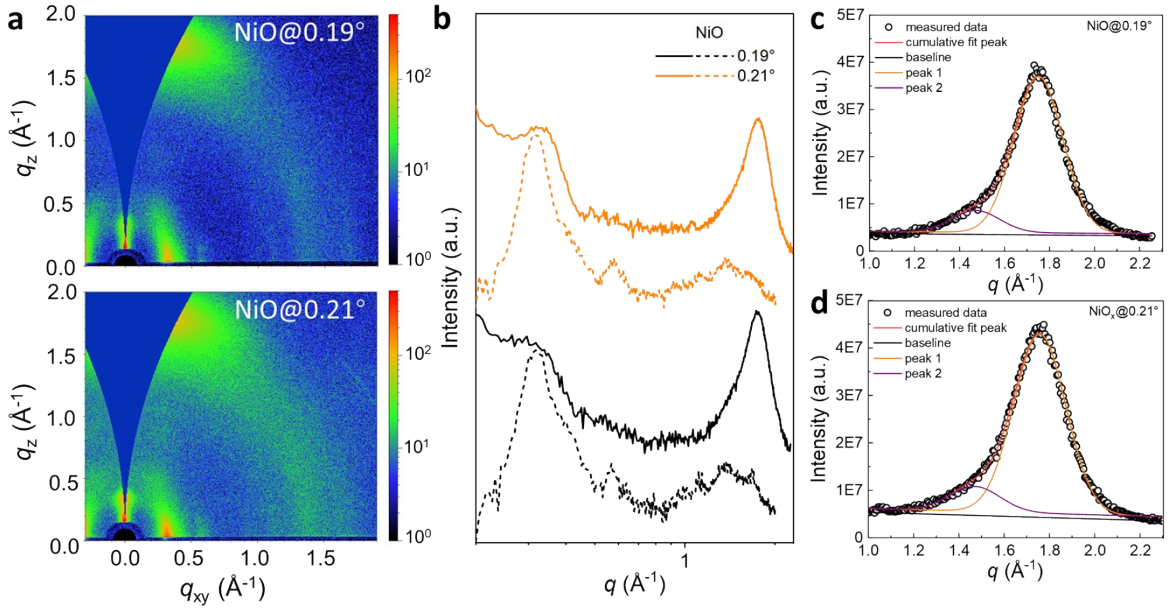

Figure S12. a. 2D GIWAXS patterns, **b.** corresponding 1D line-cue profiles and **c-d.** fitting results of at different X-ray incident angles for PBQx-TCl:eC9-2Cl coated on NiO HTL.

Table S5. Detailed GIWAXS peak information of PBQx-TF:eC9-2Cl films coated on various HTLs.

HTL	$\theta_{incident}$ (°)	$q_{Peak\ 1}$ (Å^{-1})	$q_{\pi-\pi}$ (Å^{-1})	$d_{\pi-\pi}$ (Å)	FWHM (Å^{-1})	CCL (Å)	area (*10^5)	h (nm)	area/h (10^5 nm^{-1})
PEDOT:PSS	0.19	1.402	1.705	3.685	0.287	19.70	5.355	107	0.050
	0.20	1.408	1.702	3.692	0.284	19.91	4.710	107	0.044

	0.21	1.396	1.710	3.674	0.279	20.27	4.004	107	0.037
	0.19	1.435	1.723	3.647	0.279	20.27	6.406	106	0.060
PEDOT:PSS:NiO	0.20	1.426	1.725	3.642	0.278	20.34	6.972	106	0.066
	0.21	1.443	1.724	3.645	0.277	20.41	6.025	106	0.057
	0.19	1.472	1.751	3.588	0.255	22.18	8.970	108	0.083
NiO	0.20	1.481	1.759	3.572	0.265	21.34	9.838	108	0.091
	0.21	1.470	1.757	3.576	0.270	20.94	10.866	108	0.101

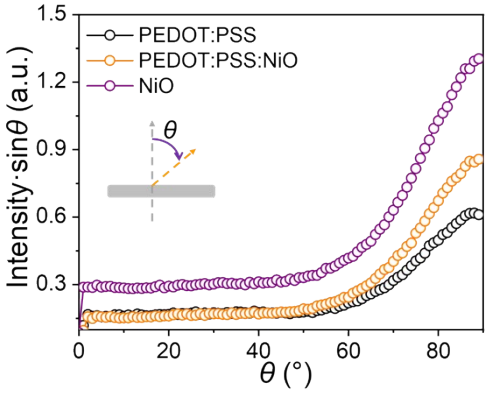

Figure S13. Corrected pole figures extracted from the π-π stacking (010) diffraction peak for the blended films. Definition of polar angle (θ) and the ranges corresponding to face-on (A_2) and edge-on (A_1) crystallites are shown. θ = 0° represents edge-on orientation, and θ = 90° represents face-on orientation relative to substrate.

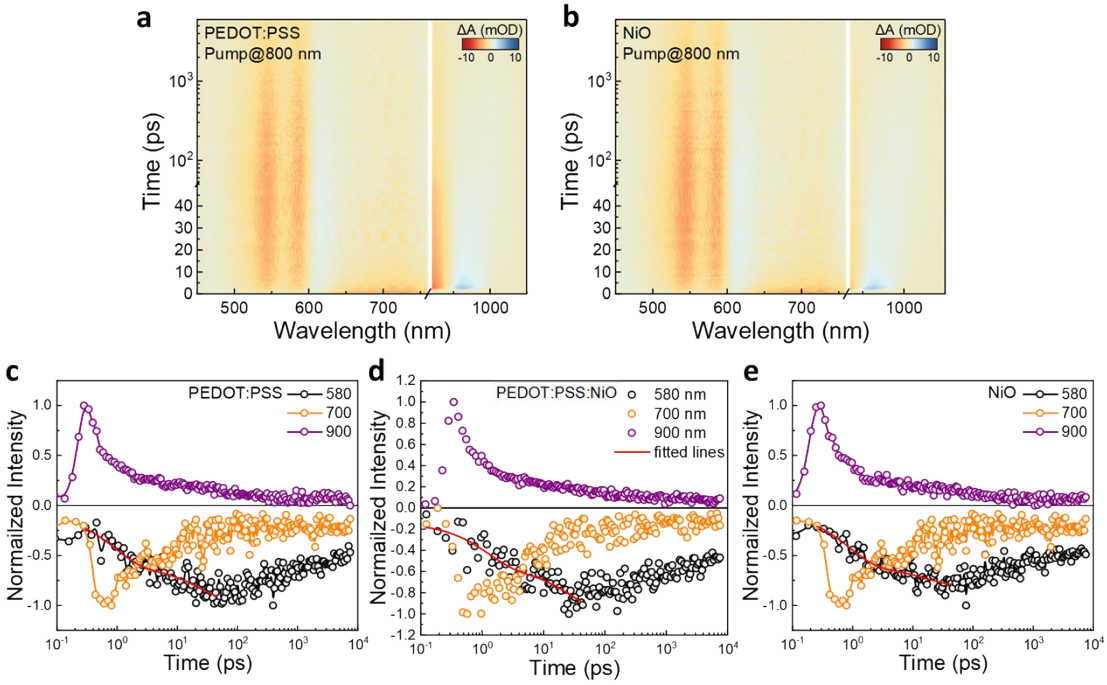

Figure S14. **a-b.** 2D TA spectra of PBQx-TCl:eC9-2Cl film coated on PEDOT:PSS and NiO, respectively, under 800 nm excitation. **c-e.** The decay dynamics of PBQx-TCl:eC9-2Cl film coated on PEDOT:PSS, PEDOT:PSS:NiO and NiO, respectively, probed at 580 nm, 700nm and 900 nm.

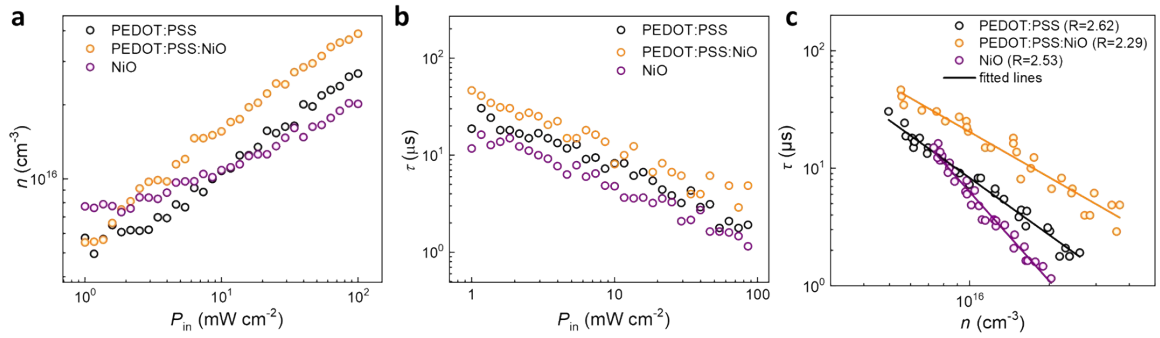

Figure S15. a. charge carrier density (n) and **b.** charge carrier lifetime (τ) under various light intensity. **c.** τ as a function of n in three OPV cells.

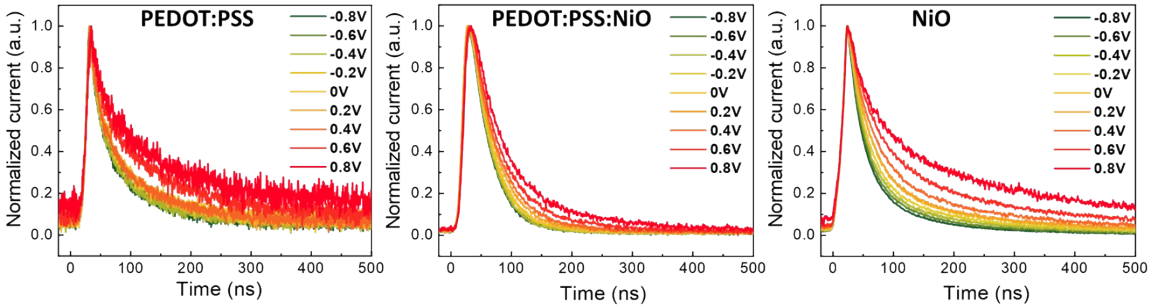

Figure S16. Transient photocurrent decay kinetics of PBQx-TCl:eC9-2Cl cells with PEDOT:PSS, PEDOT:PSS:NiO and NiO HTLs at different bias voltage.

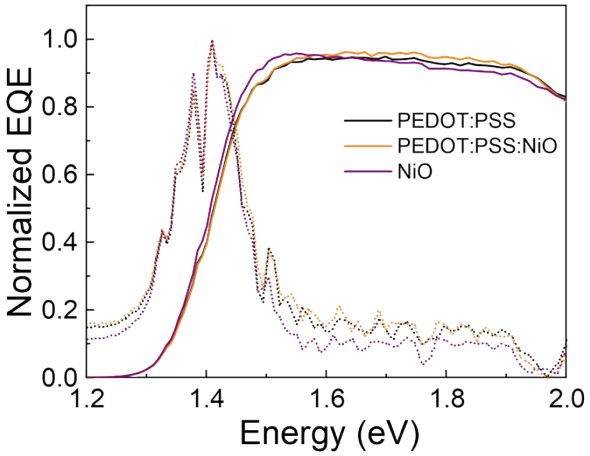

Figure S17. Optical band gap ($E_{g,opv}$) distributions for the three PBQx-TCl:eC9-2Cl cells with PEDOT:PSS, PEDOT:PSS:NiO and NiO HTLs. $E_{g,\ opv}$s are determined from the derivatives of the EQE spectra.

Table S6. Detailed energy losses of the three OPV cells bas.

HTL	$E_{g,opv}$ (eV)	qV_{OC} (eV)	qV_{loss} (eV)	$qV_{OC,\ SQ}$ (eV)	$qV_{OC,\ rad}$ (eV)	$q\Delta V_1$ (eV)	$q\Delta V_2$ (eV)	$q\Delta V_3$ (eV)	$q\Delta V_3$ (eV)[b]
PEDOT:PSS	1.419	0.888	0.531	1.153	1.108	0.266	0.045	0.220	0.231

PEDOT:PSS:NiO	1.419	0.900	0.519	1.153	1.113	0.266	0.040	0.213	0.213
NiO	1.411	0.761	0.658	1.146	1.083	0.265	0.063	0.330	0.329

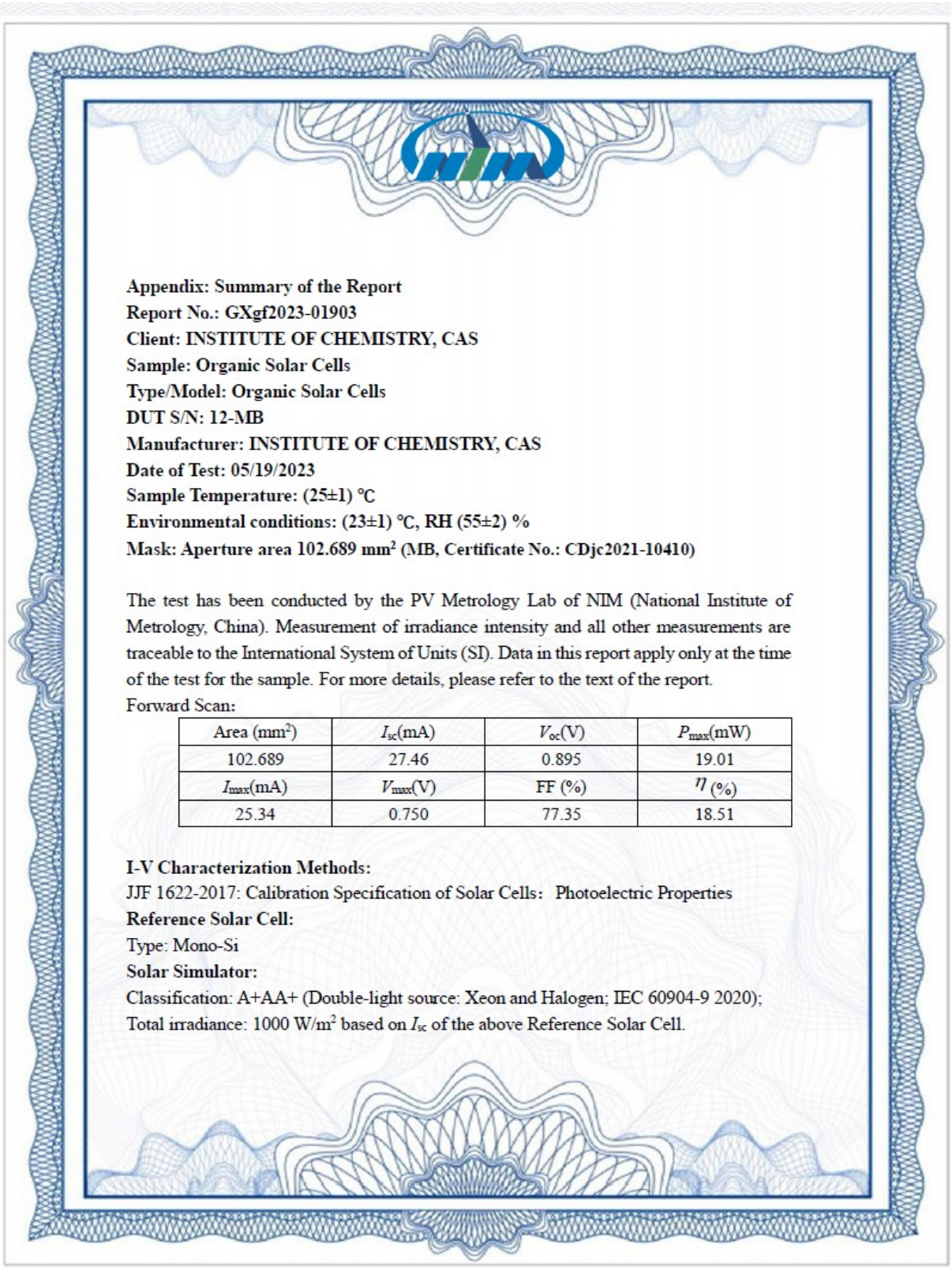

Appendix: Summary of the Report
Report No.: GXgf2023-01903
Client: INSTITUTE OF CHEMISTRY, CAS
Sample: Organic Solar Cells
Type/Model: Organic Solar Cells
DUT S/N: 12-MB
Manufacturer: INSTITUTE OF CHEMISTRY, CAS
Date of Test: 05/19/2023
Sample Temperature: (25±1) ℃
Environmental conditions: (23±1) ℃, RH (55±2) %
Mask: Aperture area 102.689 mm² (MB, Certificate No.: CDjc2021-10410)

The test has been conducted by the PV Metrology Lab of NIM (National Institute of Metrology, China). Measurement of irradiance intensity and all other measurements are traceable to the International System of Units (SI). Data in this report apply only at the time of the test for the sample. For more details, please refer to the text of the report.

Forward Scan:

Area (mm^2)	I_{sc}(mA)	V_{oc}(V)	P_{max}(mW)
102.689	27.46	0.895	19.01
I_{max}(mA)	V_{max}(V)	FF (%)	η (%)
25.34	0.750	77.35	18.51

I-V Characterization Methods:
JJF 1622-2017: Calibration Specification of Solar Cells: Photoelectric Properties
Reference Solar Cell:
Type: Mono-Si
Solar Simulator:
Classification: A+AA+ (Double-light source: Xeon and Halogen; IEC 60904-9 2020);
Total irradiance: 1000 W/m² based on I_{sc} of the above Reference Solar Cell.

Figure S18. The certification report of the best performance ternary cell based on PBQx-TCl:eC9-2Cl blade coated on PEDOT:PSS:NiO processed from NIM, China. The device area is 1.03 cm^2.

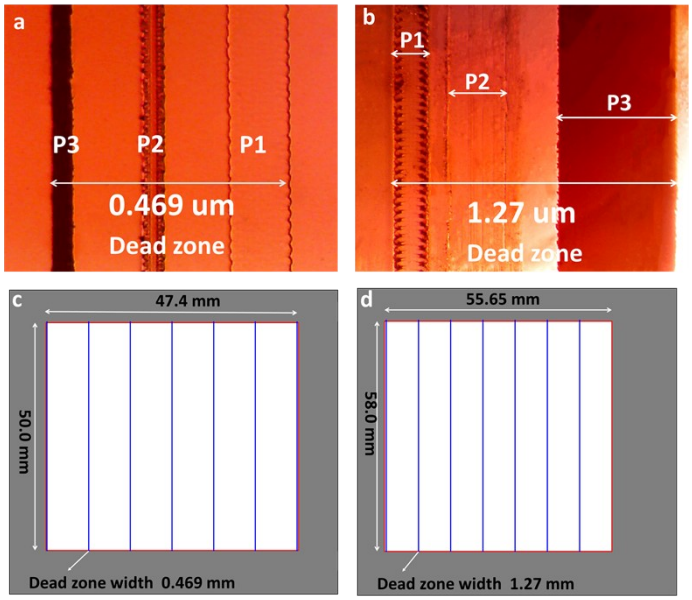

Figure S19. a-b. Bright-field microscope images of P1, P2, and P3 zones of the rigid and flexible OPV modules. The P1 (ITO) are etched by laser, and the P2 (interface layer and active layer) and P3 (electrode) are patterned by using the physical scribe. **c-d.** A schematic illustration of the dimension of the scribed rigid and flexible OPV modules. The gray area means mask, the blue lines are dead area.

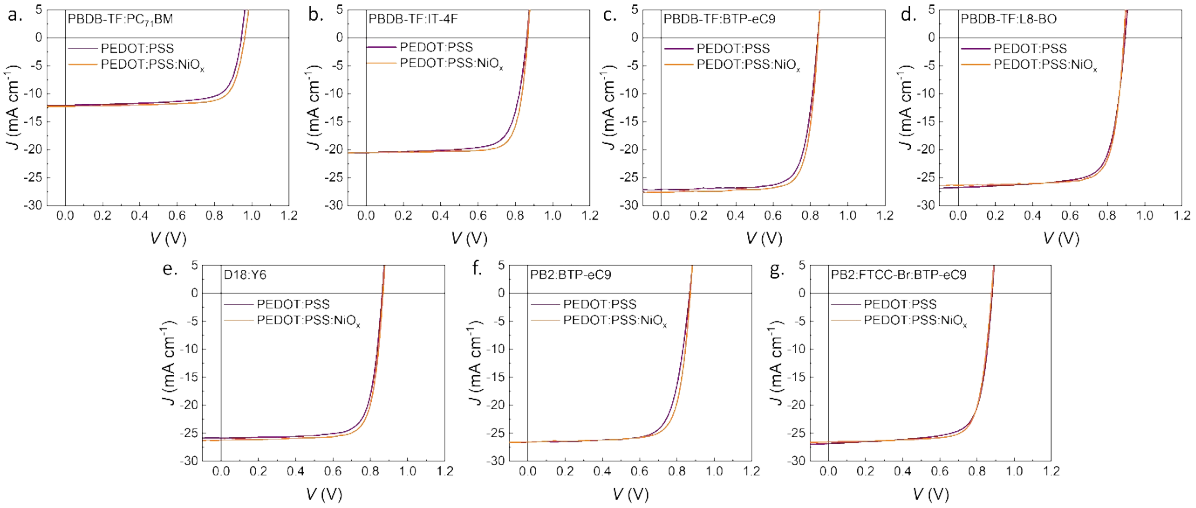

Figure S20. The *J-V* curves of PEDOT:PSS and PEDOT:PSS:NiO based OPV cells with various highly efficient active layer systems.

Table S7. The parameters of PEDOT:PSS and PEDOT:PSS:NiO based OPV cells with various highly efficient active layer systems.

Active layer	HTL	V_{OC} (V)	J_{SC} (mA cm^{-1})	FF (%)	PCE (%)
PBDB-TF:$PC_{71}BM$	PEDOT:PSS	0.942	12.1	73.5	8.36
	PEDOT:PSS:NiO	0.961	12.3	76.6	9.02

PBDB-TF:IT-4F	PEDOT:PSS	0.861	20.6	74.5	13.1
	PEDOT:PSS:NiO	0.864	20.5	79.2	14.0
PBDB-TF:BTP-eC9	PEDOT:PSS	0.838	27.1	75.9	17.3
	PEDOT:PSS:NiO	0.841	27.7	77.3	18.0
PBDB-TF:L8-BO	PEDOT:PSS	0.888	26.8	73.7	17.5
	PEDOT:PSS:NiO	0.888	26.4	77.4	18.1
D18-Cl:Y6	PEDOT:PSS	0.862	25.9	76.5	17.0
	PEDOT:PSS:NiO	0.867	26.2	78.1	17.7
PB2:BTP-eC9	PEDOT:PSS	0.867	26.6	73.7	17.0
	PEDOT:PSS:NiO	0.870	26.5	76.4	17.7
PB2:FTCC-Br-BTP-eC9	PEDOT:PSS	0.871	26.9	74.2	17.4
	PEDOT:PSS:NiO	0.877	26.8	76.9	18.1

References

[1] Y. Yu, J. Wang, Y. Cui, Z. Chen, T. Zhang, Y. Xiao, W. Wang, J. Wang, X. T. Hao, J. Hou, *J Am Chem Soc* **2024**, *146*, 8697.

[2] R. H. Perry, D. W. Green, J. O. Maloney, "Perry's Chemical Engineers' Handbook", 2007.